PHYSICAL REVIEW B **89**, 174102 (2014)

Symmetry and defects in rhombohedral single-crystalline $Na_{0.5}Bi_{0.5}TiO_3$

Richard Beanland* and Pam A. Thomas†
Department of Physics, University of Warwick, Coventry CV4 7AL, United Kingdom
(Received 20 December 2013; revised manuscript received 23 April 2014; published 8 May 2014)

Recent work has indicated that the symmetry of the lead-free piezoelectric perovskite $Na_{0.5}Bi_{0.5}TiO_3$ can be changed from monoclinic to rhombohedral through the application of an electric field, which may have implications for the study and design of piezoelectric materials close to a morphotropic phase boundary. We have examined high-quality, single-crystal $Na_{0.5}Bi_{0.5}TiO_3$ using transmission electron microscopy and have used digital electron diffraction to observe the symmetry of defect-free regions of material on length scales of a few nanometers. This unequivocally demonstrates that the material is rhombohedral with space group $R3c$ on this length scale. We find that a model that allows disordered displacements of Bi atoms from their nominal sites in the $R3c$ symmetry, while retaining this symmetry on average, gives a very significant improvement in fit to simulations. We use conventional transmission electron microscopy to enumerate the different types of defects that are observed in other regions of the crystal and find a complex microstructure of antiphase boundaries, domain walls, and tetragonal platelets. Their interaction leads to the formation of very high densities of nanotwins. We show that these are expected to have a variable monoclinic Cc symmetry that is driven by the constraint of continuity of the crystal across a domain wall.

DOI: 10.1103/PhysRevB.89.174102 PACS number(s): 61.66.Fn, 64.70.kp, 77.84.Cg

I. INTRODUCTION

The lead-free piezoelectric perovskite $Na_{0.5}Bi_{0.5}TiO_3$ (NBT) is widely promoted as one of the main components in several environmentally friendly piezoelectric materials [1–9]. Nevertheless, understanding of this material remains elusive, and even definitive classification of its space group has proved difficult. The initial neutron diffraction study of a sample consisting of flux-grown crystals crushed to produce a powder [1] yielded an $R3c$ perovskite symmetry with antiphase $a^-a^-a^-$ tilting (in Glazer notation [10]) of the oxygen octahedra from Rietveld refinement of the data. However, in this study, it was apparent that Bi, confined by the $R3c$ symmetry to a single site on the threefold axis, was severely underbonded. Subsequent studies have confirmed that there are Bi-O bond lengths that are significantly shorter (~2.2 Å) than the nominal $R3c$ symmetry allows (~2.5 Å) [11–13]. Recently, using reverse Monte Carlo (RMC) modeling of neutron diffraction data, Keeble *et al.* [12] found a split Bi-O pair distribution function which varied with temperature, also indicating displacements which are inconsistent with a rhombohedral symmetry. Other studies have found that polycrystalline or powder samples of NBT produce x-ray data that is better fit to an $a^-a^-c^-$ Cc monoclinic symmetry [13] or mixed $R3c$ and Cc [5,8,14]. Aksel *et al.* [15], using x-ray and neutron diffraction, were able to repeat the RMC result of Keeble, as well as showing that the departures from an average structure were larger in calcined in comparison with sintered material and that variations over different length scales were present in the data. Interestingly, Rao *et al.* have shown recently that application of a strong electric field (poling) can produce an irreversible transformation from mixed $R3c + Cc$ to solely $R3c$ phase as measured by x-ray diffraction [5,6,8], although they were unable to distinguish between the presence of a bulk Cc phase and the adaptive diffraction that would give diffraction akin to a Cc phase, which is the result of a high density of nanotwins [16]. Ma *et al.* have used selected area electron diffraction (SAED) of sintered NBT pellets to distinguish between $R3c$ and Cc symmetries and confirmed the presence of the Cc symmetry in heavily twinned, unpoled material [7]. Their technique relies on the presence or absence of superstructure reflections in the diffraction patterns and is unaffected by adaptive diffraction effects. In a transmission electron microscopy (TEM) study, Levin and Reaney [17] proposed a more complex pseudorhombohedral model of locally variable octahedral rotations in order to explain the presence of weak spots in electron diffraction patterns that indicate the presence of in-phase tilting of the oxygen octahedra [2,17–20]. Their model used assemblages of nanoscale orthorhombic domains that exhibited $a^-a^-c^+$ tilting, where the in-phase tilting was maintained only over lengths of a few nanometers, while antiphase tilting was maintained over longer distances to give an average $a^-a^-a^-$ or $a^-a^-c^-$ tilting over the scale probed by x-ray diffraction.

Most recently, Rao *et al.* performed a comprehensive study using x-ray, neutron, and electron diffraction as well as Raman spectroscopy and first-principles calculations [21]. They presented evidence to support the view that the application of an electric field suppresses the variable nanoscale in-phase tilting proposed by Levin and Reaney, converting NBT from a relaxor to a normal ferroelectric, and showed that heating to >300 °C was necessary to reinstate the monoclinic state upon cooling. These observations raise interesting questions concerning the origin, nature, and stability of the spatial variations in structure and symmetry. For example, do changes induced by the application of an electrical field to NBT change symmetry occur at the unit cell level or over length scales of a few nanometers (i.e. changes that could be considered to truly different phases), or is a change in the microstructure produced, giving diffraction data that is best fit by a different average symmetry? Microstructure clearly has a significant part to play, as the work of Aksel *et al.* has highlighted the

*r.beanland@warwick.ac.uk
†p.a.thomas@warwick.ac.uk

difference between sintered and calcined materials. There is a fundamental difference between these two possibilities; the first implies that there are several crystal structures that have similar energies, and the material can be switched from one to another, while the second would require defective material to have a different symmetry from that of defect-free material.

We tackle this question here by examining unpoled single crystals of NBT prepared using a flux growth technique [1] using TEM. We use computer control to obtain new types of electron diffraction data [22] from defect-free material (on the scale of a few nanometers) to give an unequivocal determination of symmetry. This is followed by an investigation of the defect microstructure of unpoled material. The results show that the average symmetry of bulk NBT is $R3c$ even in unpoled material, although (disordered) deviations from this symmetry on the unit cell level are required to match the data. We also show that the observed defect symmetry would be expected to produce a material with monoclinic Cc symmetry when averaged over large volumes of material.

II. RESULTS

A. Symmetry determination using digital electron diffraction

The basis of the technique of Ma *et al.* [7] is illustrated in Fig. 1, and uses the result that $h/2,k/2,l/2$ (h, k, l all odd integers), or ½ *ooo* superstructure reflections are absent in diffraction patterns taken along a direction perpendicular to the oxygen octahedral tilt axis [23]. For symmetry $R3c$, half of the $\langle 110\rangle_{PC}$ patterns, where the subscript PC refers to the axes of the pseudocubic perovskite cell of side ~4 Å, have no superstructure spots, whereas for symmetry Cc, spots are absent in only one of the six patterns. Thus, a statistical approach may be used, which is based on the rarity of the pattern which does not contain superstructure spots in symmetry Cc. This approach clearly assumes that there is no

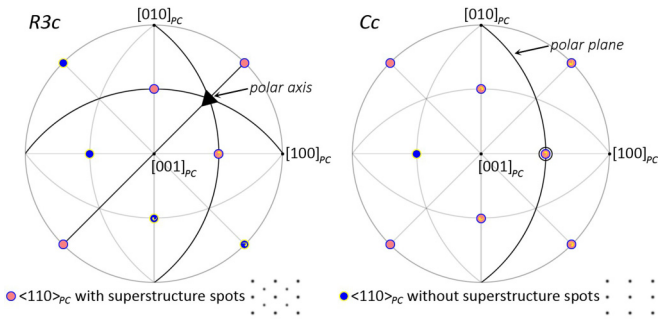

FIG. 1. (Color online) Stereographic projections looking along the pseudocubic $[001]_{PC}$ axis showing the point symmetry elements of the $R3c$ and Cc structures. Mirror (glide) planes are marked by solid lines, and the threefold axis in $R3c$ is marked by a triangle. $\langle 110\rangle_{PC}$ SAED patterns can be classified as with (red with blue line) or without (solid blue) ½ *ooo* superstructure spots. In symmetry $R3c$, all $\langle 110\rangle_{PC}$ patterns with superstructure spots have a mirror, and all $\langle 110\rangle_{PC}$ patterns without superstructure spots have symmetry 1. In symmetry Cc, only one $\langle 110\rangle_{PC}$ pattern, which also has superstructure spots, has a mirror (circled at $[101]_{PC}$), and all $\langle 110\rangle_{PC}$ patterns related to that pattern by $\{110\}_{PC}$ twin planes must also have superstructure spots but no mirror (commas). See also Figs. S1 and S2 [27].

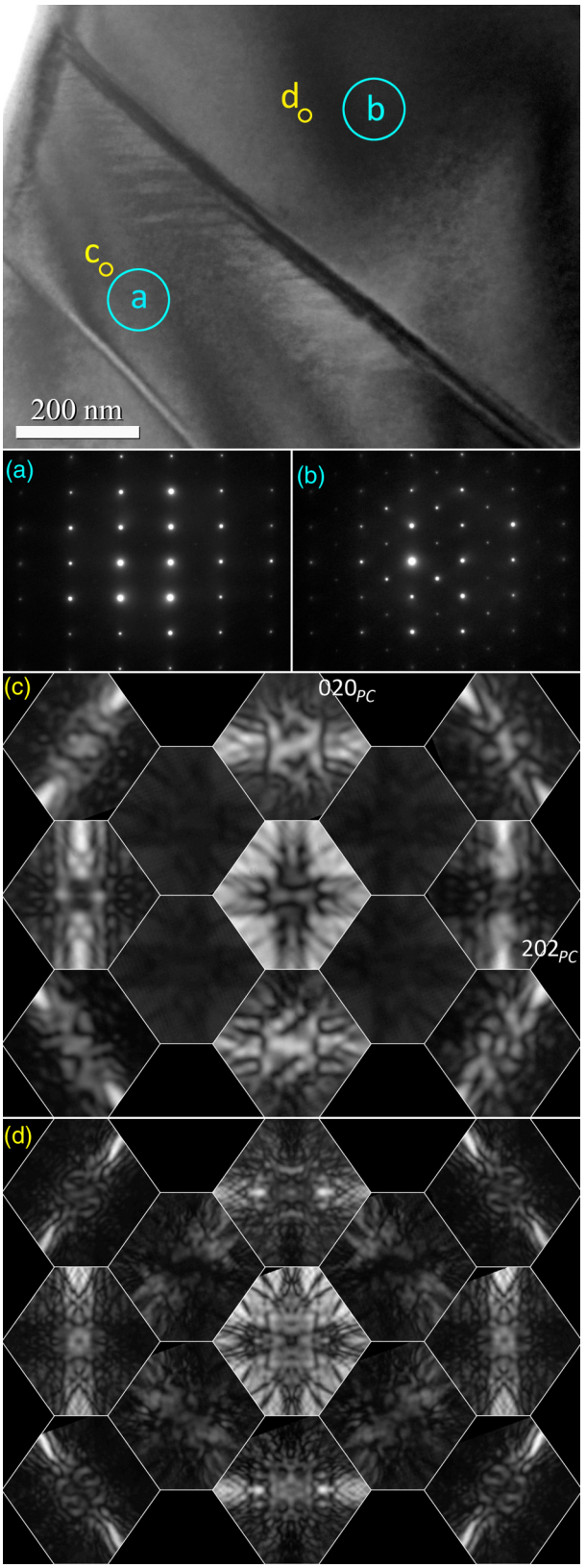

FIG. 2. (Color online) Diffraction patterns taken along a pseudocubic $\langle 101\rangle_{PC}$ axis on different sides of a $\{011\}_{PC}$ domain wall at the sites indicated. The domain wall is inclined at 45° to the beam direction. $\langle 101\rangle_{PC}$ SAED patterns (a) without and (b) with ½ *ooo* superstructure spots. (c) and (d) show D-LACBED patterns (c) with symmetry 1 and (d) with $\{110\}_{PC}$ mirror symmetry.

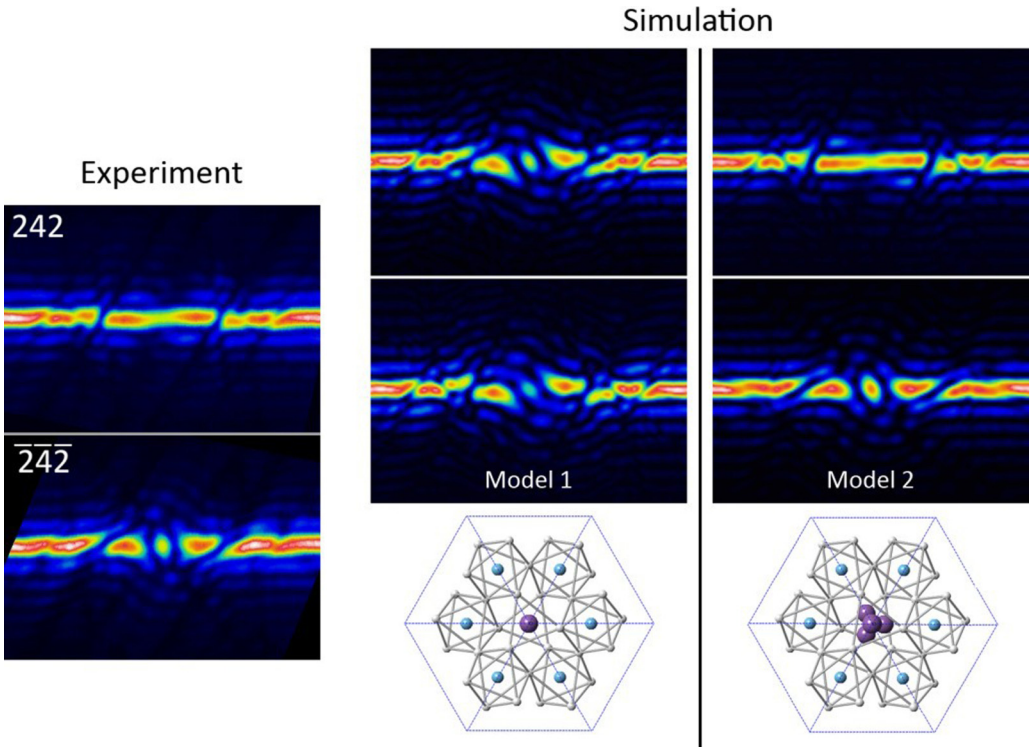

FIG. 3. (Color online) A $\pm\mathbf{g}$ pair of D-LACBED patterns, 242 and −2-4-2, taken from defect-free $Na_{0.5}Bi_{0.5}TiO_3$ at a $[-321]_{PC}$ zone axis (see Fig. S3 [27]). Simulated patterns using dynamical diffraction theory [35] are shown for the *R3c* Jones and Thomas symmetry [1] and a modified average *R3c* symmetry with disordered Bi displacements off $[111]_{PC}$ [12].

reorientation of polarization in the thin TEM specimen that would affect these probabilities. Ma *et al.* also noted that, in the case of domains with $\{100\}_{PC}$ (twinning) domain walls, the presence of superstructure spots in electron diffraction patterns for the two different $\langle 110\rangle_{PC}$ directions in the plane of the domain wall only occurs in symmetry *Cc*. Based on the presence of these spots in two such patterns, they assigned the symmetry of their $Na_{0.5}Bi_{0.5}TiO_3$ to be *Cc*, although they did not rule out the possibility of a mixed phase $Cc + R3c$ material.

The information in SAED patterns is limited in comparison with other forms of electron diffraction which allow the measurement of dynamical diffraction effects, such as convergent beam electron diffraction (CBED) [24]. However, CBED can be difficult to apply to materials which have even a moderate lattice parameter, since the angle between adjacent diffracted beams decreases in inverse proportion to the lattice parameter, and the amount of information which can be reliably extracted becomes smaller. Recently, we have developed a new technique which uses computer control of a transmission electron microscope to capture many individual CBED patterns at different angles of incidence and recombine them into a single dataset [22]. These digital large-angle CBED (D-LACBED) patterns allow unambiguous measurements of symmetry, such as the presence of mirror planes or a center of symmetry, and are used here to study $Na_{0.5}Bi_{0.5}TiO_3$. They are interpreted using the well-established rules for standard CBED patterns, first developed by Buxton *et al.* [24].

A first-principles CBED study to determine symmetry would typically require tilting of the crystal in order to obtain diffraction patterns at several low-index zone axes [25]. The insight of Ma *et al.* was to use the geometry of twinning to describe the relationship between different patterns, reducing the need to examine exactly the same region of material at several orientations, which would typically require TEM with a high tilt ($>\pm 30^\circ$) goniometer. Nevertheless, as they used SAED spot patterns, they were unable to eliminate the need for tilting completely and needed to access two different $\langle 110\rangle_{PC}$ directions, 90° apart, to give an unequivocal answer. This is still not a trivial exercise to undertake, since a region can vary significantly in appearance at different orientations, and—due to spherical aberration in the electron microscope—the region of material that actually produces a SAED pattern may be displaced from its apparent location [26]. Here, we find that the additional information that is present in D-LACBED patterns allows us to determine symmetry from two well-defined regions, each a few nanometers in size, on either side of a domain wall and without any tilting of the crystal.

In our material, we found that $\{100\}_{PC}$ domain walls were extremely rare, preventing a similar approach to that of Ma *et al.* [7]. However, $\{110\}_{PC}$ domain walls were common (and often mobile under the electron beam). In order to distinguish between *R3c* and *Cc* symmetries when $\{110\}_{PC}$ domain walls are present, we consider Fig. 1 in more detail (see also Figs. S1 and S2 in the Supplemental Material [27]). We consider the $\{110\}_{PC}$ domain walls to be twin planes, i.e. the crystal on one side of the domain wall is a broken symmetry-related orientational variant of the crystal on the other side, in this case, a reflection. There are obvious differences—for example, the presence of three mirror (glide) planes in *R3c* and only one

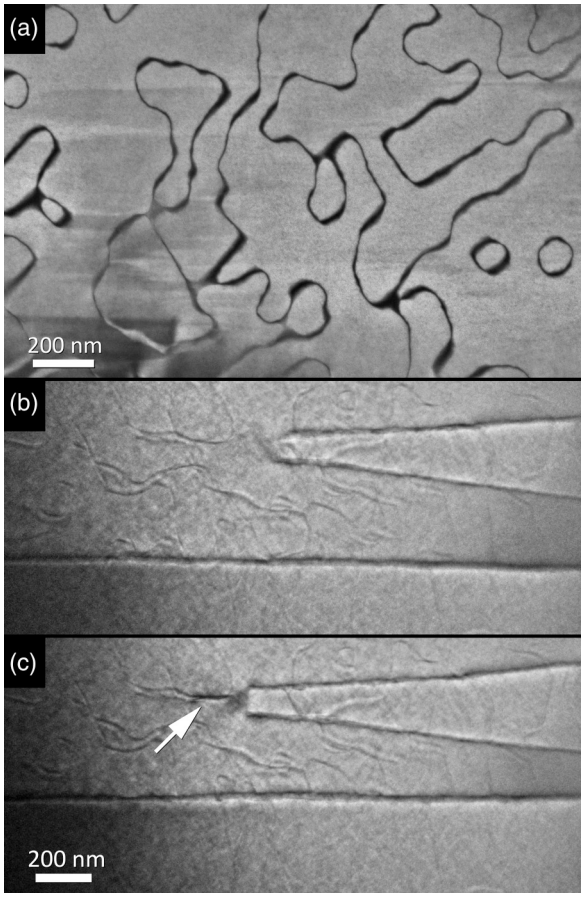

FIG. 4. (a) Transmission electron microscopy images from thin (specimen thickness $t < 40$ nm) $Na_{0.5}Bi_{0.5}TiO_3$ showing antiphase domain walls (dark field, $\mathbf{g} = 113$), (b) and (c) a wedge-shaped domain, bounded by $\{110\}_{PC}$ domain walls, moving under the influence of the electron beam and interacting with APBs to produce a nanotwin (arrowed; bright field, $\mathbf{g} = 220$).

mirror (glide) in *Cc*. Furthermore, because of the lower order of the point group (*m*) of *Cc*, more twin-related variants exist in this than in *R*3*c*.

In symmetry *R*3*c*, all $\langle 110\rangle_{PC}$ patterns with ½ *ooo* superstructure spots lie on a mirror (glide) plane, while those that have no superstructure spots do not. For any given $\langle 110\rangle_{PC}$ pattern, there are three twin-related patterns that can be found by crossing three different $\{110\}_{PC}$ domain walls, and only one of these three is of the same type (Fig. S1 [27]). In contrast, for symmetry *Cc*, only one $\langle 110\rangle_{PC}$ direction lies in the mirror-glide plane, marked by a circle in Fig. 1, and this pattern has both a mirror and exhibits superstructure spots. However, in this case, there are five twin-related patterns, and all of them have superstructure spots but no mirror (Fig. S2 [27]). It is possible to have twin-related $\langle 110\rangle_{PC}$ patterns that are of different types in *Cc* (e.g. viewed along $[-101]_{PC}$ and $[011]_{PC}$) but neither of them exhibit a mirror. Thus, the ability to distinguish between patterns (i) with and without mirror symmetry, and (ii) with and without superstructure spots, gives several ways to distinguish between *R*3*c* and *Cc* symmetries, (which we assume here are the only two possibilities to consider). For example:

(1) if a $\langle 110\rangle_{PC}$ pattern has superstructure spots and no mirror, the symmetry must be *Cc*;

(2) if two twin-related $\langle 110\rangle_{PC}$ patterns have both superstructure spots and a mirror, the symmetry must be *R*3*c*;

(3) for a $\langle 110\rangle_{PC}$ pattern with no superstructure spots, the twin-related $\langle 110\rangle_{PC}$ pattern must have superstructure spots for both *R*3*c* and *Cc*. If it has no mirror, the symmetry must be *Cc* (by condition 1); if it has a mirror, the symmetry must be *R*3*c*.

In our experiment, the crystal was grown using a flux growth technique [1], and TEM specimens were prepared using conventional methods, i.e. mechanical grinding and polishing to a thickness of approximately 20 μm, followed by Ar^+ ion milling to electron transparency and were examined in JEOL 2000FX and 2100 electron microscopes operating at 200 kV. Images were recorded using Gatan Orius digital cameras. Figure 2 shows an experimental measurement of symmetry at a $\langle 110\rangle_{PC}$ zone axis on either side of a $\{110\}_{PC}$ domain wall. Care was taken to ensure that the regions chosen for analysis were defect-free. Selected area electron diffraction patterns (a) and (b) show that the twin-related $\langle 110\rangle_{PC}$ patterns are of opposite type. The central 13 D-LACBED patterns, taken from the sites indicated on either side of the domain wall, are shown in (c) and (d). Digital large-angle CBED was performed using computer control of the JEOL 2100 TEM using a Gatan Digital Micrograph script (see Ref. [22] for more details). Figures 2(b) and 2(c) are composites of 1681 individual CBED patterns, and each pane covers an angular range larger than that of the SAED pattern. The lack of any mirror is readily apparent in (c), as expected for both *R*3*c* and *Cc* structures. Furthermore, the difference between $\pm\mathbf{g}$ patterns is very obvious (e.g. the 020_{PC} pattern is not the same as the $0\text{-}20_{PC}$ pattern). This is consistent with the absence of a center of symmetry [24], as expected for a ferroelectric polar material. Condition (3) indicates that pattern (d) should have a mirror in the case of *R*3*c*, and have no mirror in the case of *Cc*. Simple inspection of the patterns reveals that a vertical mirror is indeed present in (d), confirming the symmetry of our defect-free $Na_{0.5}Bi_{0.5}TiO_3$ to be rhombohedral *R*3*c* by condition (3) above.

Nevertheless, we find in general that dynamical simulations of our D-LACBED patterns using the original *R*3*c* model of Jones and Thomas [1] fail to reproduce the structure or detail of the experimental patterns. This is in contrast with simulations of well-known materials, where a very high degree of correspondence between experiment and simulation can be obtained [22]. As an example, we show the $\pm\mathbf{g}$ pair of reflections from a $[-321]_{PC}$ zone axis in Fig. 3 (see also Fig. S3 [27]). Significant differences exist between the experimental 242 and −2-4-2 patterns, consistent with an acentric symmetry. Simulated patterns are also shown, obtained using the *R*3*c* Jones and Thomas structure [1] (Model 1), with a single Bi atom, and a modified *R*3*c* symmetry using the structure obtained by reverse Monte Carlo fit to neutron diffraction data of Keeble [12] (Model 2). In this model, the Bi atoms occupy multiple positions, consistent with monoclinic polarization on a unit cell level, while the average structure remains consistent with an *R*3*c* symmetry. (We have not considered the additional rotations of oxygen octahedra that may be induced by these Bi displacements. In

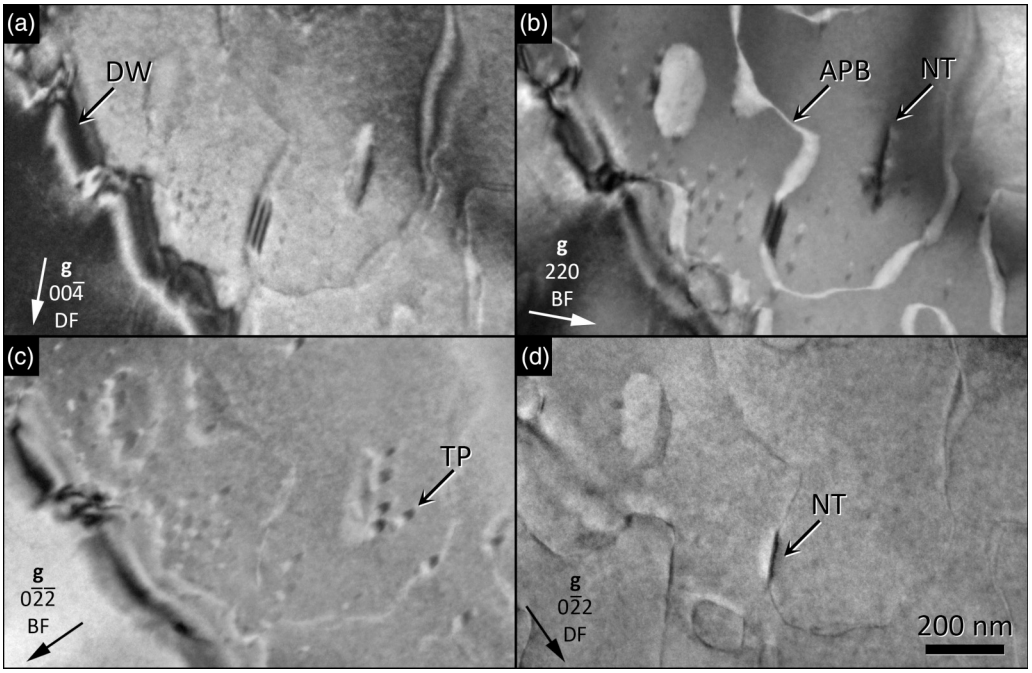

FIG. 5. Transmission electron microscopy images showing defect structures in $Na_{0.5}Bi_{0.5}TiO_3$ (specimen thickness $t \sim 60$ nm) under different two-beam diffraction conditions. (a) $\mathbf{g} = 00\text{-}4_{PC}$ and (b) $\mathbf{g} = 220_{PC}$ are taken close to the $[1\text{-}10]_{PC}$ zone axis. (c), $\mathbf{g} = 0\text{-}2\text{-}2_{PC}$ and (d) $\mathbf{g} = 0\text{-}22_{PC}$ are taken close to the $[100]_{PC}$ zone axis. DW = domain wall; APB = antiphase boundary; TP = tetragonal platelet [4]; NT = nanotwins. Note that the nanotwins are invisible for $\mathbf{g}$ vectors perpendicular to $\langle 110\rangle_{PC}$, consistent with rhombohedral twinning that is described by a shear along $\langle 110\rangle_{PC}$.

the Levin and Reaney model [17], these are locally $a^-a^-c^+$, $a^-c^+a^-$, and $c^+a^-a^-$, but globally $a^-a^-a^-$, which might also be consistent with this work.) Model 1 only produces small differences in the $\pm\mathbf{g}$ pair—and is clearly quite different from the experimental data. By contrast, Model 2 reproduces all the main features and details of the experimental data. This electron diffraction study therefore supports the concept of an average $R3c$ symmetry, which nevertheless contains local atomic displacements to satisfy the bonding valence requirements of Bi.

B. Defect structures in $Na_{0.5}Bi_{0.5}TiO_3$

This diffraction study was only possible because the prepared TEM specimens of our single-crystal material contain many square microns of thin material (specimen thickness $t < \sim 50$ nm). In fact, we find that all mobile domain walls are expelled from very thin areas, leaving only a network of sessile antiphase boundaries (APBs) as shown in Fig. 4(a). These meandering boundaries must form closed surfaces and have some tendency to lie on or close to $\{100\}_{PC}$ and $\{110\}_{PC}$ planes. An inhomogeneous distribution of small $\{100\}_{PC}$ platelets also remains [invisible in Fig. 4(a)]. These latter defects exhibit δ fringes [28] under certain imaging conditions, consistent with platelets of tetragonal $a^-a^-c^+$ material [4]. We note that this microstructure appears rather different from that seen in polycrystalline ceramics [17,20].

Domain walls with $\{110\}_{PC}$ orientations are often found to be mobile in thin, relatively defect-free material [e.g. Figs. 4(b) and 4(c)]. These have wedge-shaped morphologies, typical of ferroelectric domain structures [29]. Interactions between the domain walls and the APBs can be seen to occur (see also Fig. S4 and Video V1 in the Supplemental Material [27]). In Fig. 4(b), progress of the wedge-shaped domain from right to left is blocked by its interaction with an APB lying almost perpendicular to the $\{110\}_{PC}$ domain walls, blunting the tip of the domain. In Fig. 4(c), the domain has overcome this

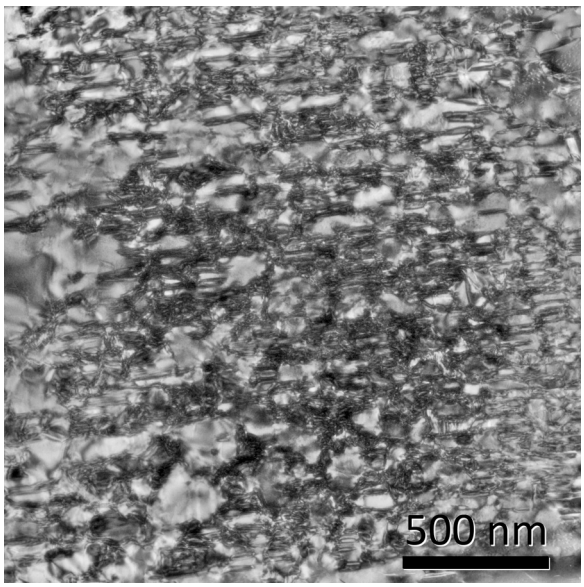

FIG. 6. Transmission electron microscopy image of the defect structures in $Na_{0.5}Bi_{0.5}TiO_3$ in a thicker part of the specimen ($t \sim$ 500 nm, $\mathbf{g} = 220_{PC}$). A very high density of nanotwins is present, decorating every APB.

TABLE I. Local symmetries at planar defects in an $a^-a^-a^-$ perovskite [3].

	Twin $\{110\}_{PC}$	APB $\{uvw\}_{PC}$	Twin +APB $\{110\}_{PC}$	Twin $\{001\}_{PC}$	APB $\{001\}_{PC}$	Twin +APB $\{001\}_{PC}$
Interface symmetry	$a^-a^-c^0$	$a^0a^0a^0$	$a^0a^0c^-$	$a^-a^-c^+$	$a^0a^0c^+$	$a^-a^-c^0$
Local symmetry[a]	$a^-a^-\alpha^-$	$\alpha^-\alpha^-\alpha^-$	$\alpha^-\alpha^-a^-$	$a^-a^-a^-$	$\alpha^-\alpha^-a^-$	$a^-a^-\alpha^-$

[a]For the local symmetry, α (where $\alpha < a$) is used to indicate octahedral tilts that are smaller than the bulk value.

obstacle and is attracted by an APB that lies almost parallel to it. A plateletlike domain (a nanotwin, NT), only a few nanometers thick, is formed on the APB (arrowed). In slightly thicker regions of the TEM specimen ($50 < t < 200$ nm), these are found more frequently (Fig. 5) and are presumably formed by the passage of a domain wall through an APB at some point in the past. Both $\{110\}_{PC}$ [Fig. 5(b)] and $\{100\}_{PC}$ [Fig. 5(d)] NTs can be observed. Note also in these images that the tetragonal $a^-a^-c^+$ platelets (TPs) are visible under some diffraction conditions. Bulk material ($t > 500$ nm) contains a very high density of NT defects (Fig. 6), where every APB is continuously decorated with nanotwins.

III. DISCUSSION

These observations not only demonstrate the complexity of NBT, but also allow several of the different experimental observations to date to be brought together in a coherent and consistent manner.

Access to clean, defect-free material is possible in the electron microscope since regions only a few nanometers in size are required for analysis. All of our data are consistent with the notion that the average bulk symmetry of NBT is rhombohedral, $R3c$ even while individual unit cells may have Bi displacements which are not along $[111]_{PC}$. Furthermore, differences from the bulk structure are clearly visible, in the form of tetragonal platelets and planar boundaries such as APBs and domain walls.

The tetragonal platelets demonstrate the local disorder that is to be expected in such a mixed A-site perovskite. The dimensions of these regions are consistent with incommensurate modulations observed using neutron diffraction [30] and diffuse contrast seen in x-ray diffraction [31,32]. They may also be responsible for the relaxor behavior of NBT [9,33]. Using density functional theory calculations, Gröting *et al.* [9] found that the different possible configurations of Na and Bi on their sublattice may favor different cation displacements and octahedral tilting on a unit cell level [9], constrained to an average symmetry only by crystal continuity. Both $a^-a^-a^-$ and $a^-a^-c^+$ structures were found to be low-energy configurations, and $a^-a^-c^+$ regions were found to be stable in sheets up to 3 unit cells thick. This is in good agreement both with the dimensions of the TPs as seen in Figs. 4(b) and 4(c) and the thickness of planar zones derived from diffuse scattering data by Kreisel *et al.* [32].

The interaction between domain walls and APBs is driven by the differences in local octahedral tilt structure, which must be present at planar defects [2,3]. If continuity of the oxygen octahedra is maintained across a planar defect in a tilted perovskite, the local octahedral tilt system around the planar defect must differ from the bulk. The local octahedral tilt systems are summarized in Table I for an $a^-a^-a^-$ perovskite. The rigidity of the octahedral network may be expected to generate a gradual transition from the local structure to the bulk, and we find that these transitional regions will have a local symmetry with general form $a^-a^-c^-$, illustrated in Fig. 7 for $\{110\}_{PC}$ domain walls. Table I shows that this is

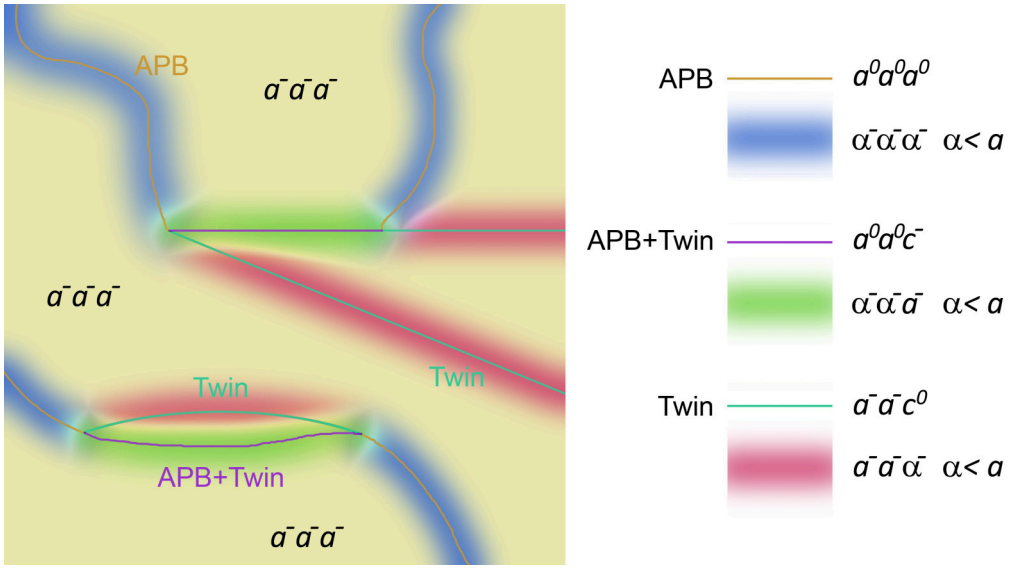

FIG. 7. (Color online) Schematic showing local octahedral tilting around $\{110\}_{PC}$ domain walls which interact with APBs. Material in the vicinity of the domain walls has $a^-a^-c^-$ tilting of variable magnitudes.

also the case for $\{100\}_{PC}$ domain walls, i.e. twinning not only is expected to give adaptive peaks in x-ray diffraction that correspond to a symmetry *Cc*, which occur even if the material is actually rhombohedral, but also the structural continuity of the oxygen octahedra constrains material adjacent to the twin boundary to actually adopt symmetry *Cc* as well. This may explain the result of Ma *et al.* [7].

Since the local structures of the different types of domain wall are different, it is inevitable that they will have a different energy per unit area γ. Since antiphase tilts cannot be maintained across an APB, the octahedral tilting must pass through zero ($a^0a^0a^0$) at the boundary and $\gamma_{(\mathrm{APB})}$ might be expected to be relatively large (confirmed by the density functional calculations of Gröting *et al.* [9]). Certainly, $\gamma_{(\mathrm{APB})}$ may be expected to be large in comparison with a $\{110\}_{PC}$ twin, which is coincident with an APB, where at least one of the tilt systems can be maintained without interruption across the boundary, and the local structure is ($a^0a^0c^-$). Neglecting strain energies which arise from domain geometries, if

$$\gamma_{(\mathrm{APB})} > \gamma_{(\mathrm{Twin})} + \gamma_{(\mathrm{Twin+APB})}, \quad (1)$$

the reaction seen in Fig. 3(d) will be energetically favorable, and the production of nanotwins as observed in bulk material (Fig. 5) is likely to occur. Furthermore, interactions between domain walls and the $a^-a^-c^+$ TPs are also likely since the different tilt systems will have a significant impact on their energy. This model is also consistent with observations of material subject to repeated cycling of electric fields, which drives domain wall motion and thus may be expected to generate more and more nanotwins decorating APBs and TPs, leading to pinning, deactivation of mobile domain walls, and fatigue [34].

The observation that unpoled material contains a high density of defects with locally different symmetries provides a consistent explanation for the experimental observations described here using TEM and also give a framework to interpret results obtained by x-ray diffraction [5,6,8]. In particular, it is to be expected that sufficiently high-poling fields will convert material from multiple domains (and therefore variably polarized) into a single domain, i.e. will remove the high density of nanotwins observed in unpoled bulk material. Large-scale diffraction measurements, which give an average measurement of the symmetry, should see a corresponding change from monoclinic $a^-a^-c^-$ to rhombohedral $a^-a^-a^-$, as observed by Rao *et al.* [5,6,8].

IV. SUMMARY AND CONCLUSIONS

We have used D-LACBED, a novel transmission electron diffraction technique, to demonstrate that defect-free NBT has an average *R*3*c* symmetry on length scales of a few nanometers. Utilizing the twinning relationship between regions on different sides of a domain wall, we have obtained an unequivocal answer from a pair of measurements, made with no tilting of the specimen. Simulations of 242-type D-LACBED patterns are consistent with a disordered structure that allows sufficiently short (~2.2 Å) Bi-O bonding, as observed in earlier local structure measurements [11,12,32]. Conventional TEM analysis of defect types in bulk NBT reveals a complex structure of antiphase boundaries (APBs), tetragonal platelets (TPs), and domain walls. We find that the high energy of APBs, due to their incompatibility with antiphase tilting of the oxygen octahedra, attracts domain walls to lie in coincidence with them, resulting in the formation of very high densities of nanotwins, a few unit cells wide, in bulk material. We note that material in the vicinity of these defects will generally adopt a variable $a^-a^-c^-$ structure as a transition between the local symmetry at the defect and the bulk, and speculate that their elimination by the application of a high electric field may be the cause of the irreversible change in symmetry seen in recent x-ray studies [5,8].

ACKNOWLEDGMENTS

This work was funded by the EPSRC under Grant No. EP/J009229/1. One of the Gatan Orius digital TEM cameras used in this research was funded by the Advanced Materials (1) project: Creating and Characterising Next Generation Advanced Materials, part funded by Advantage West Midlands and the European Regional Development Fund.

[1] G. O. Jones and P. A. Thomas, Acta Crystallogr. Sect. B **58**, 168 (2002).
[2] V. Dorcet, G. Trolliard, and P. Boullay, J. Magn. Magn. Mater. **321**, 1758 (2009).
[3] R. Beanland, Acta Cryst. **A67**, 191 (2011).
[4] R. Beanland and P. A. Thomas, Scr. Mater. **65**, 440 (2011).
[5] B. N. Rao and R. Ranjan, Phys. Rev. B **86**, 134103 (2012).
[6] R. Garg, B. N. Rao, A. Senyshyn, P. S. R. Krishna, and R. Ranjan, Phys. Rev. B **88**, 014103 (2013).
[7] C. Ma, H. Guo, and X. Tan, Adv. Funct. Mater. **23**, 5261 (2013).
[8] B. N. Rao, A. N. Fitch, and R. Ranjan, Phys. Rev. B **87**, 060102 (2013).
[9] M. Gröting, I. Kornev, B. Dkhil, and K. Albe, Phys. Rev. B **86**, 134118 (2012).
[10] A. Glazer, Acta Crystallogr. Sect. B **28**, 3384 (1972).
[11] V. A. Shuvaeva, D. Zekria, A. M. Glazer, Q. Jiang, S. M. Weber, P. Bhattacharya, and P. A. Thomas, Phys. Rev. B **71**, 174114 (2005).
[12] D. S. Keeble, E. R. Barney, D. A. Keen, M. G. Tucker, J. Kreisel, and P. A. Thomas, Adv. Funct. Mater. **23**, 185 (2013).
[13] E. Aksel, J. S. Forrester, J. L. Jones, P. A. Thomas, K. Page, and M. R. Suchomel, Appl. Phys. Lett. **98**, 152901 (2011).
[14] S. Gorfman, A. M. Glazer, Y. Noguchi, M. Miyayama, H. Luo, and P. A. Thomas, J. Appl. Crystallogr. **45**, 444 (2012).
[15] E. Aksel, J. S. Forrester, J. C. Nino, K. Page, D. P. Shoemaker, and J. L. Jones, Phys. Rev. B **87**, 104113 (2013).
[16] Y. U. Wang, Phys. Rev. B **76**, 024108 (2007).
[17] I. Levin and I. M. Reaney, Adv. Funct. Mater. **22**, 3445 (2012).
[18] V. Dorcet, G. Trolliard, and P. Boullay, Chem. Mater. **20**, 5061 (2008).

[19] I. Levin, I. M. Reaney, E. M. Anton, W. Jo, J. Rödel, J. Pokorny, L. A. Schmitt, H. J. Kleebe, M. Hinterstein, and J. L. Jones, Phys. Rev. B **87**, 024113 (2013).
[20] V. Dorcet and G. Trolliard, Acta Mater. **56**, 1753 (2008).
[21] B. N. Rao, R. Datta, S. S. Chandrashekaran, D. K. Mishra, V. Sathe, A. Senyshyn, and R. Ranjan, Phys. Rev. B **88**, 224103 (2013).
[22] R. Beanland, P. J. Thomas, D. I. Woodward, P. A. Thomas, and R. A. Roemer, Acta Crystallogr. Sect. A **69**, 427 (2013).
[23] D. I. Woodward and I. M. Reaney, Acta Crystallogr. Sect. B **61**, 387 (2005).
[24] B. F. Buxton, J. A. Eades, J. W. Steeds, and G. M. Rackham, Philos. Trans. R. Soc. London A **281**, 171 (1976).
[25] J. P. Morniroli, G. Ji, and D. Jacob, Ultramicroscopy **121**, 42 (2012).
[26] P. B. Hirsch, A. Howie, R. B. Nicholson, D. W. Pashley, and M. J. Whelan, *Electron Microscopy of Thin Crystals* (Robert E Krieger Publishing Co. Inc., Malabar, FL, 1977).
[27] See Supplemental Material at http://link.aps.org/supplemental/10.1103/PhysRevB.89.174102 for additional figures and video.
[28] D. B. Williams and C. B. Carter, *Transmission Electron Microscopy: A Textbook for Materials Science*, 2nd ed. (Springer Verlag, New York, 2009).
[29] M. E. Lines and A. M. Glass, *Principles and Applications of Ferroelectrics and Related Materials* (Oxford University Press, Oxford, 1977).
[30] A. M. Balagurov, E. Y. Koroleva, A. A. Naberezhnov, V. P. Sakhnenko, B. N. Savenko, N. V. Ter-Oganessian, and S. B. Vakhrushev, Phase Transitions **79**, 163 (2006).
[31] P. A. Thomas, S. Trujillo, M. Boudard, S. Gorfman, and J. Kreisel, Solid State Sci. **12**, 311 (2010).
[32] J. Kreisel, P. Bouvier, B. Dkhil, P. A. Thomas, A. M. Glazer, T. R. Welberry, B. Chaabane, and M. Mezouar, Phys. Rev. B **68**, 014113 (2003).
[33] N. Setter and L. E. Cross, J. Appl. Phys. **51**, 4356 (1980).
[34] H. Simons, J. Glaum, J. E. Daniels, A. J. Studer, A. Liess, J. Rödel, and M. Hoffman, J. Appl. Phys. **112**, 044101 (2012).
[35] P. A. Stadelmann, Ultramicroscopy **21**, 131 (1987).